Effect of tortuosity on the diffusion of polystyrenes through porous materials with diff erent architectures

Khac Long Nguyen, Véronique Wernert, André Morgado Lopes, Loïc Sorbier,
Renaud Denoyel

HAL Id: hal-02447627
https://ifp.hal.science/hal-02447627

Effect of tortuosity on the diffusion of polystyrenes through porous materials with different architectures

Khac-Long Nguyen[a,b], Véronique Wernert[a], André Morgado Lopes[a,c], Loïc Sorbier[c], Renaud Denoyel[a]

a) Aix-Marseille Université, CNRS, MADIREL UMR 7246, 13397 Marseille cedex 20, France

b) Hanoi University of Mining and Geology, 18 Vien Street, Bac Tu Liem, Hanoi, Vietnam

c) IFP Energies nouvelles, Rond-point de l'échangeur de Solaize, BP 3, 69360, Solaize, France

Corresponding author:

Véronique Wernert

e-mail address: veronique.wernert@univ-amu.fr

Tel: +33 4 13 55 18 40

1

Abstract

The tortuosity parameter, essential in the prediction of molecular transport properties, is determined on several materials with multiscale porosities: interparticular/interskeletal macropores and intraparticular/intraskeletal mesopores for beds of spherical porous particles and monoliths. Electrical measurements (impedance spectroscopy) and peak parking experiments are used. The former measures the electrical resistance between two electrodes surrounding the porous material impregnated with concentrated electrolyte, while the latter uses a set of polystyrene molecules in non-adsorbing conditions within a chromatographic setup. Tortuosity measurements as well as characterization via mercury porosimetry, nitrogen adsorption and inverse size exclusion chromatography (ISEC) are performed on four materials: fully porous silica and alumina particles, porous-shell silica particles and silica monoliths. The tortuosity determined by electrical measurements is in agreement with peak parking with the smallest probe (toluene). The particle tortuosity is 1.6 and 1.8 for fully porous silica and alumina particles respectively and 2.3 for porous-shell silica particles. For molecules which size is not negligible as compared to pore size, the intraparticle diffusion coefficient can be estimated from the hindrance factor, which can be calculated with the Renkin correlation and the apparent particle tortuosity for the considered probe. The latter is estimated from the Weissberg equation $\tau_p[r_m]=1-p\ln(\varepsilon_p[r_m])$, where $\varepsilon_p[r_m]$ is the particle porosity accessible to a molecule of size r_m and p a parameter depending on the material topology. A model with just one adjustable parameter p can thus estimate the intraparticle diffusion coefficient.

Keywords: peak parking, effective diffusion coefficient, intraparticle diffusion coefficient, tortuosity, Maxwell equation

1. Introduction

A better understanding of transport through porous materials has become very important for the effective design, preparation and production of columns in the separation and catalysis fields. For example silica columns with different morphologies are used for the separation of molecules: totally porous particles, core-shell particles or monoliths are available. γ-aluminas are used as catalyst supports in refinery processes such as cuts petroleum hydroprocessing. The mass transfer properties are very important in the activity of the catalyst [1]: the diffusion of the molecules and especially heavy liquid petroleum fractions in the pore network of alumina is the limiting step in the processes and it is often necessary to adapt the pore organization to increase the efficiency. The tortuosity of a porous material is a useful parameter to evaluate a-priori the influence of pore morphology on the easiness of transport. It can be measured from diffusion or electrical experiments. One of the ways to measure the effective diffusion coefficient (D_{eff}) in a column is the analysis of band broadening at very slow elution speed or at zero flow rate by keeping the eluent for a given time in a column, which is depicted as arrested elution or peak parking (PP) method initially reported by Giddings and Knox [2, 3, 4, 5]. In this method, the molecule is arrested in the column far enough from the extremities by stopping the pump during a given time called the parking time (t_p) where the molecule can freely diffuse through the porous media. The pump is then restarted and the dispersion of the molecule during this time is recorded. The effective diffusion coefficient (D_{eff}) is obtained from the Einstein's diffusion equation by measuring the variance of the peak in unit length ($\Delta \sigma_z^2$) for a given parking time t_p [4, 6]:

$$\Delta \sigma_z^2 = 2 D_{eff} t_p \tag{1}$$

To determine the intraparticle diffusion coefficient from the global effective diffusion coefficient obtained from equation 1 it is necessary to use models such as Effective Medium Theory (EMT) models. EMT expressions can be found in the literature about the effective electrical and thermal conductivities of packings of spheres and monoliths. The predictions of the EMT models are better than those obtained with the residence time weighted (RTW) expression because this latter model is based on the additivity of the mass fluxes in each phase. Among EMT models, there are implicit and explicit models. The Landauer-Davis model considers the solid skeleton as a set of microscopic inhomogeneities dispersed randomly in the bulk mobile phase, however, this implicit model fails to describe the diffusion results [7]. Among the explicit models, the Maxwell model is the most simple and is sufficient to describe the effective diffusion in non-adsorbing [7] and adsorbing conditions [8, 9], despite the fact that this model is valid only for diluted concentration of heterogeneities [10]. Models like the Torquato model, which considers near-neighbor interactions, do not better predict satisfactorily the experimental results [7]. The Maxwell equation is widely accepted in the field of chemical engineering to represent the diffusion in packed bed columns. The Maxwell model can be

extended to the porous-shell particles [8, 9, 11] and monoliths [8, 9, 12]. It has also been used to determine the particle tortuosity of spherical particles by electrical measurements using the suspension dilution method for which the model is rigorously applicable [13]. In this study, the Maxwell equation has been used to determine the intraparticle diffusion coefficient (D_p) from a peak parking measurement and the particle tortuosity by electrical measurements using the suspension dilution method.

In non-adsorbing conditions, the intraparticle diffusion coefficient of molecules, whose size is not negligible as compared to pore size, depends on the accessible porosity ($\varepsilon_p[r_m]$), the friction between the molecule and the pore wall ($k_f[r_m]$), which has to be taken into account when the size of the molecule r_m increases, and the tortuosity (τ_p) or the obstruction factor ($\gamma_p = 1/\tau_p$):

$$\frac{D_p}{D_m} = \frac{\varepsilon_p[r_m]k_f[r_m]}{\tau_p} \tag{2}$$

The friction coefficient can be calculated by using the Renkin equation [14]:

$$k_f[r_m] = 1 - 2.10\frac{r_m}{r_p} + 2.09\left(\frac{r_m}{r_p}\right)^3 - 0.95\left(\frac{r_m}{r_p}\right)^5 \tag{3}$$

where r_m is the size of the molecule and r_p is the pore size. For conductivity experiments $k_f[r_m]$ is close to 1 because the electrolyte is very small as compared to the pore size for systems studied here and this term is generally not considered for the calculation of the tortuosity by electrical measurements. In this model two points deserve further scrutiny. The first is about the value of the tortuosity, which is often considered as a constant property of the porous network with values ranging between 1.4 and 2 whatever the size of the molecule. The value of tortuosity is mainly measured by NMR [15, 16] or by electrical conductivity [13, 17, 18, 19] using probes having a size negligible as compared to the pore size. For other sizes, it is reasonable to speak of "apparent tortuosity". The second point concerns the intraparticle porosity which is used in the calculation of the intraparticle diffusion coefficient. In the PP method the molecule is already in the porosity when the pump is stopped, and the diffusion is thus only hindered by tortuosity and friction with the pore walls and not by accessibility. Equation 1 is thus questionable. In order to clarify those points, the effective diffusion of polystyrenes of different sizes has been determined in non-adsorbing conditions through commercial columns filled with silica or alumina by using the PP method. For silica, the columns are composed of totally porous particles, porous-shell particles or monoliths. For alumina only totally porous particles are used. The total, external (corresponding to macropores) and internal (corresponding to mesopores) tortuosities are determined from the effective diffusion coefficients obtained for toluene and a series of polystyrenes by the PP method and compared to the values obtained by electrical measurements in order to validate the model used in the calculation of the intraparticle diffusion coefficient in the EMT models. The effect of the size of the molecule on the total and intraparticle apparent tortuosities is determined by the PP method.

4

2. Theory

The Maxwell model is used in this study to determine the intraparticle diffusion coefficient of polystyrenes of different sizes in columns filled with silica with different morphologies and alumina, starting from total diffusion coefficient in the column. The Maxwell model is also used for the determination of the tortuosity by electrical measurements.

2.1 Maxwell model for spherical particles

2.1.1 Fully porous particles

The Maxwell expression for the effective electrical conductivity (σ_{eff}) of a suspension of particles is written as [13, 17]

$$\frac{\sigma_{eff}}{\sigma_m} = \frac{1 + 2\beta(1 - \varepsilon_e)}{1 - \beta(1 - \varepsilon_e)} = \frac{\varepsilon_t}{\tau_t} \tag{4}$$

where σ_m is the conductivity of the medium surrounding the particles, ε_e and ε_t are the external and total porosities and τ_t is the total tortuosity. The parameter β depends only on the particle conductivity σ_p:

$$\beta = \frac{\frac{\sigma_p}{\sigma_m} - 1}{\frac{\sigma_p}{\sigma_m} + 2} = \frac{\frac{\varepsilon_p}{\tau_p} - 1}{\frac{\varepsilon_p}{\tau_p} + 2} \tag{5}$$

where ε_p is the particle porosity and τ_p the particle tortuosity.

The Maxwell model is also used to determine the effective diffusion by replacing the electrical conductivity by diffusion coefficient [8]. The equivalence between conductivity and diffusion is [8]:

$$\sigma_{eff} \equiv \varepsilon_t D_{eff} \tag{6}$$

and thus

$$\frac{D_{eff}}{D_m} = \frac{1}{\varepsilon_t} \cdot \frac{1 + 2\beta(1 - \varepsilon_e)}{1 - \beta(1 - \varepsilon_e)} = \frac{1}{\tau_t} \tag{7}$$

When the size of the molecule is not negligible as compared to pore size, the tortuosity in equation 7 is an apparent tortuosity. The parameter β depends only on the ratio between the intraparticle (D_p) and the molecular diffusion (D_m) coefficients:

$$\beta = \frac{\frac{D_p}{D_m} - 1}{\frac{D_p}{D_m} + 2} \tag{8}$$

with

$$\sigma_p \equiv \varepsilon_p D_p \tag{9}$$

2.1.2 Porous-shell particles

The effect of the solid core has to be taken into account in the models. The porosity of the porous zone ε_{pz} and the particle porosity ε_p expressed on the whole particle basis are related by [8]:

$$\varepsilon_p = (1 - \rho^3)\varepsilon_{pz} \tag{10}$$

where ρ is the ratio between the core diameter (d_{core}) and the particle diameter (d'_p) ($\rho = \frac{d_{core}}{d'_p}$).

To take into account the effect of the solid core it is also important to distinguish between D_{pz} and D_p. D_{pz} is the diffusion in the meso-porous zone (entire particle in the case of fully porous particles, shell layer in case of a porous-shell particle). For spheres, the relation between D_p and D_{pz} is [8]:

$$D_p = \frac{1}{1 + \frac{\rho^3}{2}} D_{pz} \tag{11}$$

Equation 11 is obtained from the EMT models and a similar equation could be applied to conductivity:

$$\sigma_p = \frac{1}{1 + \frac{\rho^3}{2}} \sigma_{pz} \tag{12}$$

2.2 Maxwell model for monoliths

The Maxwell model has also been established for cylinder packings [8, 12] and it is assumed this is a good representation of the skeleton of monoliths. The expression is:

$$\frac{D_{eff}}{D_m} = \frac{1}{\varepsilon_t} \cdot \frac{1 + \beta(1 - \varepsilon_e)}{1 - \beta(1 - \varepsilon_e)} \tag{13}$$

and

$$\beta = \frac{\frac{D_p}{D_m} - 1}{\frac{D_p}{D_m} + 1} \tag{14}$$

2.3. Determination of D_p and D_{pz} from the effective diffusion coefficients (D_{eff}) obtained by the PP method

The values of D_p could be obtained by measuring the D_{eff} values by the PP method. The value of β can be calculated for spheres and cylinders by using equations 7 and 13 respectively to give:

$$\beta = \frac{1}{1 - \varepsilon_e} \frac{\varepsilon_t \frac{D_{eff}}{D_m} - 1}{\varepsilon_t \frac{D_{eff}}{D_m} + 2} \qquad \text{(spheres) (15)}$$

$$\beta = \frac{1}{1 - \varepsilon_e} \frac{\varepsilon_t \frac{D_{eff}}{D_m} - 1}{\varepsilon_t \frac{D_{eff}}{D_m} + 1} \qquad \text{(cylinders) (16)}$$

By knowing β, the value of $\frac{D_p}{D_m}$ can be calculated by using equations 8 and 14 to give:

$$\frac{D_p}{D_m} = \frac{1 + 2\beta}{1 - \beta} \qquad \text{(spheres) (17)}$$

$$\frac{D_p}{D_m} = \frac{1 + \beta}{1 - \beta} \qquad \text{(cylinders) (18)}$$

6

For porous-shell columns $\frac{D_{pz}}{D_m}$ is calculated by using equation 11.

3. Experimental

3.1. Columns

The columns were composed of fully porous particles made of silica (Lichrospher Si100, Merck) or alumina (Chromegasphere Alumina, ES Industries), porous-shell silica particles (Agilent) and monolithic silica (Merck). The main characteristics of the columns are given in Table I.

3.2. Chemicals

Tetrahydrofuran (THF) used as a mobile phase was purchased from Carlo Erba Reagents (SDS). Toluene was purchased from Aldrich. Twelve polystyrene standards with molecular weights M_w ranging between 162 and 1,850,000 g mol^{-1} were provided from Polymer Standards Service (Mainz, Germany). Samples of toluene and polystyrenes were dissolved in the mobile phase (THF) at a concentration of 1 g/L. The molecular diffusion coefficients (D_m) were obtained previously in THF by Taylor Dispersion Analysis (TDA) and Dynamic Light Scattering (DLS) experiments [20]. The hydrodynamic radius of the polymers (r_m) is then calculated by using the Stokes-Einstein equation. The size (r_m), molecular weight, index of polydispersity (PDI) and molecular diffusion coefficient (D_m) of toluene and of the polystyrenes from P1 to P12 are given in Table II. Detection was done at 262 nm by UV-VIS spectroscopy.

3.3. HPLC system

The experiments were made by using the 1200 HPLC system (Agilent Technologies), including a quaternary gradient pump with a multi-diode array UV-VIS detector, an automatic sample injector with a 100μL loop, an autosampler and a thermostated column compartment. The injection volume was set at 1 μL and all experiments were conducted at 298K. The system is controlled by the Chemstation software.

3.4 ISEC experiments

The porous properties and the mean pore size of the solids were determined by ISEC measurements using toluene and the polystyrene standards in THF (non-adsorbing conditions) at a flow rate of 0.5 ml min^{-1}. The chromatograms were fitted with a Gaussian function in order to evaluate the mean retention time (t_R). The total accessible volume $V_t[r_m]$ for a molecule of a given size is calculated from the mean retention time of this molecule multiplied by the flow rate. Preliminary experiments are done without column in order to evaluate the volume of the capillaries (V_a). The value of $\varepsilon_t[r_m]$ is then derived from:

$$\varepsilon_t[r_m] = \frac{V_t[r_m] - V_a}{V_c} \qquad (19)$$

where V_c is the geometrical volume of the column.

The external porosities (ε_e) were derived by extrapolating to zero hydrodynamic molecular radius the branches of ISEC plots corresponding to the accessible porosity of excluded polymers versus their molecular weight [21].

The accessible particle porosity $\varepsilon_{pz}[r_m]$ to a probe of radius r_m is estimated by the following equation [22]:

$$\varepsilon_{pz}[r_m] = \frac{\varepsilon_t[r_m] - \varepsilon_e}{(1 - \varepsilon_e)(1 - \rho^3)} \qquad (20)$$

where ε_e is the external porosity and ρ is the ratio of the solid core to the shell particle diameter. ρ=0 for totally porous particles and monolith columns and ρ=0.625 for the porous-shell column used in this study.

The determination of the pore size distribution (PSD) of mesopore zone is described in details in [23]. Briefly the pore size distribution (PSD) is calculated by fitting the experimental distribution coefficient K_d with the theoretical one.

The experimental K_d is calculated by:

$$K_d = \frac{\varepsilon_t[r_m] - \varepsilon_e}{\varepsilon_t - \varepsilon_e} \qquad (21)$$

where ε_t is the total porosity obtained with the smallest molecule, here toluene. K_d varies between 0 for a totally excluded molecule and 1 for a molecule which have access to the total pore volume (here toluene). The theoretical K_d is given by the following equation where $f(r)$ is the pore-size distribution function and $f(r)d(r)$ represents the pore volume which has a radius between r and $r+dr$ [23, 24]:

$$K_d = \frac{\int_{r_m}^{\infty} f(r)[1 - r_m/r]^2 dr}{\int_0^{\infty} f(r)dr} \qquad (22)$$

The Solver program in Excel was used to fit the model with the experimental K_d values to obtain $f(r)$. The mean pore size is determined by using the following equation:

$$\bar{r} = \frac{\int_0^{\infty} rf(r)dr}{\int_0^{\infty} f(r)dr} \qquad (23)$$

All the results are given in Table III.

3.5. Characterization of the solids by mercury porosimetry and nitrogen adsorption

After the experiments, the materials were retrieved out the columns to be characterized by mercury intrusion porosimetry and nitrogen adsorption. Mercury porosimetry experiments were carried out with the Poremaster apparatus from Quantachrome. Intrusion and extrusion are carried out after the

sample was evacuated at a pressure lower than 10 Pa. The cumulative intruded volume is measured as a function of intrusion pressure. This latter is transformed in pore size by applying the Laplace Washburn equation with a contact angle of 130°. Nitrogen sorption isotherms at 77 K were determined with an ASAP2010 apparatus from Micromeritics. The solid was outgassed overnight before analysis at a temperature of 120°C and a pressure below 1 Pa. The Brunauer–Emmett–Teller (BET) equation was applied to determine the specific surface area. Average pore diameter and pore volume have been evaluated from the nitrogen adsorption-desorption isotherms by applying the Barrett-Joyner-Halenda (BJH) model. The BJH method is based on the Kelvin equation, which defines the equilibrium pressure for capillary condensation [25].

3.6. Tortuosity determination

3.6.1 Spherical particles

The tortuosity of the particles was determined by conductivity measurements as already described [13, 19]. The particles were fluidized in a thermostated cell at 20°C in a sodium chloride solution at 1 mol L^{-1} high enough so that tortuosity is independent of salt concentration [19]. Impedance spectroscopy (from 1 kHz to 1 MHz) using a standard two-electrodes conductivity cell integrated in the fluidized bed was used to measure the electrical resistance. The amplitude of the exiting signal was fixed at 30 mV. A ModuLab® electrochemical system (Model 2101A, Solartron Analytical, UK) controlled by a personal computer using ModuLab software was used in order to separate suspension resistance from electrode effects.

The porosity of the suspension was varied by adding powders by 0.1 g increments to 30 cm^3 of electrolyte. At each step, the cumulative volume V_p of particles added to the solution was calculated by dividing the cumulative weight of dried material, m_p (in g) by the density ρ of the material:

$$V_p = \frac{m_p}{\rho_s}$$
(24)

The total porosity ε_t was then deduced by

$$\varepsilon_t = \frac{V_i}{V_i + V_p}$$
(25)

where V_i is the initial volume of the electrolyte

3.6.2 Monoliths

A voltage-controlled AC impedance experiment was performed in a thermostated bath at 20°C by applying an alternative voltage axially across the monolithic column filled with electrolyte solution (NaCl, 1 mol L^{-1}) and measuring the electrical impedance of the column. The frequency of the AC signal was varied from 1 kHz to 1 MHz using a ModuLab electrochemical system (Model 2101A, Solartron Analytical, UK). From the measured impedance, the column resistance was determined with the ModuLab software.

Due to the contribution of the dead volume in the monolithic column, a conductivity measurement of a blank column with the same length as that of the monolithic column was carried out. To eliminate the electrical resistance through the end-fitting of the monolithic and blank column, a conductivity measurement of a zero volume column was also taken into account. The stainless steel end fittings are used as electrodes.

Given the inverse relationship between resistivity and conductivity, the total tortuosity of the monolith was obtained from [13, 18]:

$$\tau_t = \varepsilon_t \frac{\sigma_m}{\sigma_{eff}} \tag{26}$$

whereas ε_t is the total porosity of monolithic, σ_{eff} is the effective conductivity of the electrolyte filled monolithic column and σ_m is the conductivity of the NaCl solution.

3.7. Peak parking (PP) experiments

The peak parking (PP) method was used to measure the apparent effective diffusion coefficient of molecules through porous media. In the PP experiments, 1 µL of a dilute sample solution was injected at 0.5 mL min^{-1}. The columns were eluted during the time necessary for the sample to arrive about half length of the column. Then the flow was stopped and the molecule left to diffuse freely during a given time called the parking time t_p. The flow was returned to the same flow rate and the peak variance of the solute band, σ_t^2, was measured. The variance of the peak is measured by fitting the chromatograms with a Gauss function. To correct for the other sources of band broadening (injector, connecting tubing) the peak variance values obtained without parking was subtracted from the peak variance values obtained with parking. The variance was then plotted versus parking time and the slope is used to calculate the effective diffusion by using the following equation:

$$D_{eff} = \frac{1}{2} \frac{\Delta \sigma_t^2}{t_p} \left(\frac{\varepsilon_e}{\varepsilon_t [r_m]} \right) u^2 \tag{27}$$

where the porosities are obtained by ISEC and u is the interstitial linear velocity.

4. Results and discussion

4.1. Characterization of the pore structure by mercury porosimetry, gas adsorption and ISEC

The samples were analyzed by mercury intrusion extrusion porosimetry. The curves are given in fig. 1a for all samples. The first step is due to the compaction of the bed, the second step corresponds to the filling of the macropores and the third step to the filling of the mesopores. In the case of spherical particles the macropores correspond to the interparticle pores, whereas for monoliths it is the interskeleton pores. The porosities are determined from these curves: the total porosity is obtained by dividing the volume of mercury intruded (V_t) which corresponds to the

difference between the volume obtained at 3 nm and the volume at the end of the first step by the total volume which is the sum of the volume of intruded mercury (V_t) and the volume occupied by the solid ($1/\rho_s$) (ρ_s=2.2 g cm^{-3} for silica and 3.6 g cm^{-3} for alumina):

$$\varepsilon_t = \frac{V_t}{V_t + 1/\rho_s} \tag{28}$$

The macroporous porosity is obtained by dividing the macroporous volume (volume of the second step) by the total volume:

$$\varepsilon_e = \frac{V_{macro}}{V_t + 1/\rho_s} \tag{29}$$

The particle porosity and skeleton porosity are obtained by dividing the mesoporous volume (volume of the third step) by the volume of the particle:

$$\varepsilon_p = \frac{V_{meso}}{V_{meso} + 1/\rho_s} \tag{30}$$

The porosities are given in table III. The external porosities obtained for the spherical particles are around 0.37 as usually found for a dense packing of spheres. It shows that after the compaction step, the compacity in mercury cell and in column are similar. The external porosity of the silica monolith is around 0.63. The particle porosities are comparable for the totally porous silica and the silica monolith around 0.64, whereas slightly lower values are obtained for the core-shell particles (0.53). The pore size distribution curves obtained from the intrusion curves are given in fig. 1b. The mean pore sizes are given in table III. In the mesoporous domain, the PSD is sharp for the porous-shell silica, monolithic silica and alumina but it is very broad in the case of the totally porous silica with two peaks at 5.5 and 14 nm. The manufacturer indicates a pore diameter around 10 nm for the totally porous silica. The samples were also characterized by nitrogen adsorption.

Nitrogen adsorption-desorption isotherms are presented in fig. 1c. The isotherms are of type IV as usually obtained for mesoporous samples. The pore size distribution obtained from the desorption branches are given in fig. 1d. Again the PSD obtained for the totally porous silica is broader than for the other solids. The pore sizes obtained by gas adsorption are close to that obtained by mercury intrusion.

The PSD is also derived from the distribution coefficient K_d obtained by ISEC. The K_d curves are presented in fig. 1e and the PSD in fig. 1f. There are less points on the PSD compared to the two other methods because a series of only 12 polystyrenes and toluene are used and only some of them enter inside mesopores. The mean pore sizes are given in table III. The mean pore sizes obtained by ISEC are higher than those obtained by gas adsorption as seen in table III but the results can be considered in good agreement given differences between methods.

The total, external and particle porosities are also determined by ISEC. The total and particle porosities determined for each polymer are plotted as a function of the ratio between the size of the

molecule (r_m) and the mean mesopore size (r_p) in figures 2a and 2b respectively. The total and particle porosities decreases as the molecular size increases. The total porosity is larger for the monolithic column than for the columns packed with the particles which is mainly due to the fact that the external porosity is higher for the monolithic column (0.69) than for the columns filled with spherical particles (around 0.4). The external porosities obtained by ISEC are comparable to the values obtained by Hg porosimetry (table III). The particle porosity obtained with the smallest molecule (*i.e.* toluene) is slightly higher for the monolithic column than for the other columns. The particle porosity values found by mercury intrusion are comparable or slightly lower than the values obtained by gas adsorption and ISEC. The difference could be explained by the presence of smaller pores (inferior to 3 nm) which can not be filled by mercury at the highest intrusion pressure applied, around 400 MPa.

4.2. Determination of particle tortuosity by conductivity measurements

When using the suspension dilution method, the total tortuosity of the suspension τ_t is calculated from the effective conductivity of the suspension σ_{eff} and from the conductivity of the electrolyte σ_m by applying eq. 26.

The Maxwell equation (eq. 4) applied to data at infinite dilution of particles is used to determine the particle conductivity (σ_p) and then the intraparticle tortuosity (τ_p). A rearrangement of the Maxwell equation by introducing eq. 26 gives:

$$\tau_t = \epsilon_t \frac{2 + \frac{\sigma_p}{\sigma_m} + (1 - \varepsilon_e)(1 - \frac{\sigma_p}{\sigma_m})}{2 + \frac{\sigma_p}{\sigma_m} - 2(1 - \varepsilon_e)(1 - \frac{\sigma_p}{\sigma_m})} \tag{31}$$

The tortuosity of the suspension is measured as a function of the porosity and modeled by eq. 31 by varying the ratio σ_p/σ_m until experimental and theoretical data are concurrent, tending towards 1 at infinite dilution. The results obtained for porous silica and alumina and porous-shell particles are given in figure 3. The tortuosity of the particles τ_p can be calculated by:

$$\tau_p = \frac{\varepsilon_p \sigma_m}{\sigma_p} \tag{32}$$

where ε_p is the particle porosity. For the porous-shell particles eq. 12 must be taken into account in order to calculate the tortuosity of the porous zone.

The particle tortuosity obtained by impedance spectroscopy are reported in table IV. The particle tortuosity can be also calculated by the following equation which is theoretically found for spheres (Weissberg) [26] and experimentally verified for some other shapes [27]:

$$\tau_p = 1 - p \ln(\varepsilon_p) \tag{33}$$

The *p* value depends on the pore topology with proposed values of *p=0.41* [27] or *p=0.49* [28] for spheres, *p=0.53* for cubes and *p=0.86-3.2* for plate [27]. This equation has been validated by both experiments [13, 20, 29] and simulations [30, 31]. The *p* value obtained by electrical measurements

are given in table IV. The justification of such approach is to consider that porous materials are often built by aggregation of small objects.

The total tortuosity of the monolith measured by electrical measurements is 1.13. This value could be compared to the value obtained from the PP method with the smallest molecule *i.e.* toluene which is 1.09. This will be discussed in the next part. The intraparticle tortuosities are 1.6 and 1.8 for totally porous silica and alumina particles respectively. The intraparticle tortuosity found for the porous-shell column is higher with a value around 2.3. The p values obtained from the Weissberg equation (eq. 33) are 1.6 and 1.3 for totally porous silica and alumina particles respectively and 2.5 for the porous-shell silica.

Kolitchev *et al.* [1] obtain particle tortuosities around 2 and 3 for columns filled with different γ-aluminas whatever the size of the molecule. They determine the intraparticle diffusion coefficient and thus the particle tortuosity from the slope of the HETP curves. They obtain higher values since they do not consider neither the friction between the molecules and the pore walls nor the accessible porosity even with the largest molecule, which is squalane ($C_{30}H_{62}$), an aliphatic compound. The aluminas they used are polydisperse due to inter and intra-aggregates porosities. The particle tortuosity found by [1] in the inter-aggregates domain is around 1.6 and 1.9, values close to the value obtained in this study.

4.3. Determination of effective diffusion coefficients D_{eff} and of total and external tortuosities by PP method

Examples of peak parking bands obtained with the columns for different parking times are presented in figures 4a and 4b for small and large molecules respectively. The peaks are symmetrical and broaden with increasing parking time which is due to diffusion. Similar results were obtained for all columns and polystyrenes studied. The curves with solid lines are the reference peak with no parking time. The variance of the peak is evaluated for each parking time to determine the effective diffusion coefficient. Firstly a linear baseline correction of the whole chromatogram is performed to correct for the baseline drift of the signal. Secondly, the chromatogram is fitted with a Gauss function. The R^2 are higher than 0.99 in all cases. The variance of the peak was calculated from the Gauss fit. The peak variance is plotted as a function of the parking time as shown in fig. 4c. It should be noticed that all the curves are straight lines in agreement with equation 1. The slope of the line decreases as the molecular size increases which is due to slower diffusion when the size of the molecule increases.

Applying equation 27, the value of effective diffusion coefficient, D_{eff}, for each probe is determined. A comparison of the ratios of D_{eff}/D_m as a function of r_m/r_p in the four columns is presented in fig. 4d. The ratio D_{eff}/D_m decreases as the molecular size increases until r_m/r_p around 0.3 due to slower

diffusion in the particles then the D_{eff}/D_m increases until a constant value which corresponds to diffusion mainly in macropores. It can be observed that this value is almost the same for the three columns made of spherical particles: the intersphere porosity is the same and the size of the polymers is small as compare to macropore size. The effective diffusion in the silica monolith column is faster than that in column packed with spherical particles which could be explained by a higher external porosity leading to higher diffusion in the macroporosity [32]. In fact the external porosity of the monolithic column is around 0.69 against 0.4 for the columns packed with spherical particles. The apparent total tortuosities of the silicas and alumina obtained from eq. 7 for spherical particles and eq. 13 for monolith are plotted in figure 5. It appears that the apparent tortuosity is smaller for the monolith than for the spherical particles. The apparent tortuosity which is a combination of the external and intraparticle tortuosities increases as the molecular size increases until $r_m/r_p=0.3$ and then decreases as the molecular size increases. For r_m/r_p larger than one the external tortuosity or the tortuosity in the macropore is obtained. The external tortuosity, *i.e.* tortuosity of the macropore is 1.05 for the monolith and 1.38 for the columns packed with spherical particles (porous-shell and totally porous silicas). The results are given in table IV. The *p* values are then calculated by the Weissberg equation using the external porosity. For packing of spheres *p=0.4* in agreement with discussion above and literature [27]. For the monolithic column *p=0.3* which appears to be small if we consider that the skeleton of monoliths has the morphology of an assembly of cylinders. For a packing of spheres values around 1.3 and 1.6 are usually obtained [30]. The tortuosity in the macropores can be calculated from the Maxwell model by applying $D_p/D_m=0$. This gives:

$$\tau_{ext} = \frac{3 - \varepsilon_{ext}}{2} \tag{34}$$

for spheres, and :

$$\tau_{ext} = 2 - \varepsilon_{ext} \tag{35}$$

for cylinders.

By using these equations the external tortuosities are around 1.3 for all the columns. This value is close to the values obtained for columns packed with spherical particles but for the monolithic column the external tortuosity obtained by PP method is smaller around 1.1. Johnson *et al* (2017) [33] determined the tortuosity in the macropores of columns packed with ceramic and cellulose by X-ray computed tomography systems and values around 1.40 and 1.79 were obtained respectively. Those values are close to the values obtained in this study by PP method. Hormann *et al* (2016) [34] determined the tortuosity of the macropores in silica monoliths by using medial axis analysis (MAA) and a geodesic distance propagation method after reconstruction of the macropores by confocal laser scanning microscopy. The global geometrical tortuosity found by [34] in the macropore is 1.09 for the silica monoliths (propagation method) and the branch tortuosity is 1.18 (MAA). The branch tortuosity is larger because the medial axis path is longer than the geodesic

distance. The diffusive tortuosity obtained by random walk is about 1.47. This value is larger than the geometrical tortuosity due to deviation from the ideal route by Brownian motion and effect of constriction in the diffusive path. The low tortuosity value obtained for monolith reflect an open macropore space that provides little obstruction to percolation. The Maxwell model overestimated the external tortuosity in the case of monoliths but calculated values are in agreement with the experimental values in the case of a packing of spherical particles.

4.4 Determination of the intraparticle diffusion coefficient and intraparticle tortuosity by the PP method

The intraparticle diffusion coefficient in the porous zone (D_{pz}) is calculated from the experimental D_{eff}/D_m values and by using the Maxwell model to separate the external contribution from the internal contribution. The D_{pz}/D_m values are reported as a function of the ratio between the size of the molecule and the pore size (r_m/r_p) for the four columns in fig. 6. The intraparticle diffusion coefficient decreases as the size of the molecule increases. For the columns packed with spherical particles the ratio D_{pz}/D_m tends to zero but for the monolithic column the value is around 0.2 for r_m/r_p close to one. This could be explained by the fact that the intraparticle diffusion coefficient is calculated from the Maxwell model which does not fit the experimental results for r_m/r_p larger than 0.3 (see fig. 4 d). Comparable diffusion coefficients are obtained, in the case of the smallest molecules, for the monolithic column and the totally porous columns. Lower values are obtained for the porous-shell column. For intermediate sized molecules the intraparticle diffusion is slightly higher for the monolithic column compared to the columns filled with spherical particles. The diffusion in the mesoporous zone has been determined by Hlushkou et al (2017) [35] by reconstructing a macroporous-mesoporous silica monolith. The void space of the amorphous mesoporous silica from the monolithic skeleton was physically reconstructed by scanning transmission electron microscopy (STEM) tomography. The effective particle diffusion coefficient in the mesopore space as a function of the size of the tracer diameter was determined by numerical simulation using a random-walk particle-tracking method. They also found a decrease of the effective diffusion by increasing the tracer size and the results are comparable to the results obtained here by the PP method. For the smallest tracer they obtain values of D_p/D_m around 0.6, values which are close to the values obtained with the smallest probe i.e. toluene in this study. They also found a decrease of D_p/D_m to values close to zero for r_m/r_p close to 0.3. The plot in fig. 6 for the monolithic column show an increase of D_{pz}/D_m for r_m/r_p larger than 0.3 instead of a decrease. This is explained by the fact that the intraparticle diffusion coefficient is calculated from the Maxwell model which overestimates the value of the tortuosity in the macropores (1.3 against 1.1 measured experimentally). Maier and Schure (2018) [36] determined the intraparticle effective diffusion in wide-pore superficially porous particles using pore-scale simulation. They found higher values of

intrapraticle diffusion coefficient around 0.6 for D_{pz}/D_m when the size of the molecule is negligible as compared to the pore size which could be explained by the fact that their materials have a pore radius around 50 nm and is probably less tortuous than the porous-shell silica used in this study.

The intraparticle tortuosity is calculated from the D_{pz}/D_m values obtained from the Maxwell model and the experimental D_{eff}/D_m values. The experimental results can be compared to the model usually used to calculate intraparticle diffusion coefficients in the PP method in non-adsorbing conditions [37]:

$$\frac{D_{pz}}{D_m} = \frac{\varepsilon_{pz}[r_m]k_f[r_m]}{\tau_{pz}} \tag{36}$$

where $k_f[r_m]$ is the friction coefficient which can be calculated by using the Renkin equation.

By applying equation 36 to the smallest molecule i.e. toluene the intraparticle tortuosity is 1.1 for porous silica and 1.6 for the porous-shell particles. Those values are lower than the values obtained by electrical measurements (see table IV). In the PP method the molecule is already present in the intraparticle porosity so the intraparticle porosity has not to be considered in the calculation of the intraparticle diffusion coefficient. The same reason is invoked to extract tortuosity from NMR measurements [38]. Thus the intraparticle tortuosity should be obtained from:

$$\tau_{pz}[r_m] = \frac{k_f[r_m]D_m}{D_{pz}[r_m]} \tag{37}$$

By using equation 37 the intraparticle tortuosity obtained for toluene is 1.6 and 1.8 for totally porous silica and alumina particles respectively and 2.7 for porous-shell particles. Those values are close to the electrical measurements where 1.6 for silica, 1.8 for alumina and 2.3 for porous-shell particles are obtained. The D_{eff}/D_m values can be calculated as reported in figure 4d by using the Maxwell equation (equations 7 and 13) and the intraparticle tortuosity and the p values obtained by electrical measurements (see table IV) or by the PP method with toluene. A good agreement is found for the porous-shell column whatever the size of the molecule by using the p value obtained with toluene but for the monolithic column there is a good agreement only until $r_m/rp=0.3$ whereas for higher values the external tortuosity is overestimated. For the fully porous particles made of silica or alumina the fit is good for the smallest and the biggest molecules but for the intermediate sized molecules ($0.1<r_m/r_p<0.6$) the fit with the p value obtained by electrical measurements is not so good. This will be explored in more details in the next part by studying the evolution of the intraparticle tortuosity with the size of the molecule. The intraparticle tortuosity in the mesoporous zone is reported in fig. 7 as a function of intraparticle porosity for the four columns. For $r_m/r_p>0.3$ the intraparticle tortuosity for spherical particles becomes very high (data not presented) because the particle diffusion becomes close to zero. The total tortuosity is thus dominated by the external tortuosity. This could explain the minimum observed in the D_{eff}/D_m curves around $r_m/r_p=0.3$. For the smallest molecule, *i.e.* toluene, the intra-particle tortuosity is around 1.6±0.1 for all the columns studied except for the porous-shell column which has a higher intraparticle tortuosity around 2.7.

Often the tortuosity is taken as a constant value whatever the size of the molecule. From fig. 7 we can see that the apparent particle tortuosity depends on the size of the molecule. When the size of the molecule increases the apparent intraparticle tortuosity increases. Such behavior has also been observed by Richard and Striegel (2010) [39]. Beckert *et al* (2010) [40] measured the molecular self-diffusion of polystyrenes solutions in porous acrylate-based monoliths by pulsed field gradient (PFG) nuclear magnetic resonance (NMR). They found a constant tortuosity around 1.5 whatever the size of the molecule, which is explained by the fact that the polystyrenes cannot enter in the mesoporosity and thus only the tortuosity in the macropores is measured in their study.

The Weissberg equation is used and extended to the accessible intraparticle porosity [7]:

$$\tau_{pz}[r_m] = 1 - p \ln\left(\varepsilon_{pz}[r_m]\right) \tag{38}$$

By using equation 38 and the value of p obtained by electrical measurements for all the columns except the monolith where the p value obtained with toluene is used (see table IV) it is possible to fit the experimental intraparticle tortuosity obtained by PP method as seen in fig. 7. There is a good agreement between the intraparticle tortuosity obtained by electrical measurements and the intraparticle tortuosity obtained with the smallest molecule. The model is correct for the porous-shell column and the monolithic column whatever the size of the molecule. For the totally porous particles the intraparticle tortuosity given by the Weissberg equation underestimate the intraparticle tortuosity of the intermediate sized molecules. For the totally porous silica column the intraparticle tortuosity is three times higher for an intermediate molecule than the value given by the Weissberg model. This could be explained by the fact that the totally porous silica particles have two types of mesopores as seen in figure 1 which could have different tortuosities. The paths followed by an intermediate sized molecule is more tortuous than the path followed by a small molecule like toluene. The constriction which is included in the tortuosity parameter has a higher influence on the diffusion for intermediate sized molecules than for smaller molecules. Another explanation could be that the Renkin equation used in this study to calculate the friction between the molecule and the pore wall overestimates the friction values $k_f[r_m]$ leading to higher intraparticle tortuosities. The Renkin equation has been obtained from experimental results and is widely used to estimate the friction coefficient but it is a parameter which is not measured usually, and the values given by this expression are highly uncertain. The effect of the friction on the diffusion must be more precisely taken into account in the future.

5. Conclusion

Transport of toluene and polystyrene compounds in non-adsorbing conditions were investigated by Peak Parking experiments on columns formed by various morphologies: fully porous silica and alumina particles, core shell porous silica and monolithic silica. A good agreement is found between

the pore size distribution and accessible porosities obtained from the retention times, nitrogen desorption and mercury intrusion. The variance of the peaks have been processed using the Maxwell equation. The intraparticle tortuosities obtained by the PP method with the smallest probe *i.e.* toluene for spherical particles or the total tortuosity obtained for monolith are comparable to the values obtained by electrical measurements provided the intraparticle diffusion coefficient is the ratio between the friction coefficient and the particle tortuosity. The molecule is already present in the porosity during the PP method, therefore, the accessible porosity has not to be considered in the calculation of the intraparticle diffusion coefficient. Using such data processing, transport of large molecules in column of rather different morphologies can be satisfactory predicted. The effect of the size of the molecule on the effective diffusion and on the apparent and intraparticle tortuosity is also shown. The apparent tortuosity increases until $r_m/r_p=0.3$ and then decreases to a constant value which is the external tortuosity or the tortuosity in the macropores. The apparent tortuosity is a subtle combination of internal and external tortuosities. This point will be studied in the future.

Acknowledgments

References

[1] S. Kolitcheff, E. Jolimaitre, A. Hugon, J. Verstraete, P.-L. Carrette, M. Tayakout-Fayolle, Mic. Mes. Mat. 248 (2017) 91-98. https://doi.org/10.1016/j.micromeso.2017.04.010

[2] J.H. Knox, L. McLaren, Anal. Chem. 36 (1964) 1477–1482. https://doi.org/10.1021/ac60214a017.

[3] J.H. Knox, J. Chromatogr. Sci. 15 (1977) 352–364. https://doi.org/10.1093/chromsci/15.9.352

[4] J.H. Knox, H.P. Scott, J. Chromatogr. A. 282 (1983) 297–313. https://doi.org/10.1016/S0021-9673(00)91609-1

[5] J.H. Knox, J. Chromatogr. A. 831 (1999) 3–15. https://doi.org/10.1016/S0021-9673(98)00497-X

[6] F. Gritti, G. Guiochon, Chem. Eng. Sci. 61 (2006) 7636–7650. https://doi.org/10.1016/j.ces.2006.08.070

[7] V. Wernert, R. Bouchet, R. Denoyel, J. Chromatogr. A. 1325 (2014) 179–185 https://doi.org/10.1016/j.chroma.2013.12.029

[8] G. Desmet, S. Deridder, J. Chromatogr. A. 1218 (2011) 32–45. https://doi.org/10.1016/j.chroma.2010.10.087

[9] S. Deridder, G. Desmet, J. Chromatogr. A. 1218 (2011) 46–56. https://doi.org/10.1016/j.chroma.2010.10.086

[10] J.C. Maxwell, A treatise on electricity and magnetism, Oxford, Clarendon Press, 1873.

[11] F. Gritti, G. Guiochon, Chem. Eng. Sci. 66 (2011) 6168–6179. https://doi.org/10.1016/j.ces.2011.08.043

[12] S. Torquato, Random Heterogeneous Materials, Springer Science & Business Media, New York, 2002.

[13] M. Barrande, R. Bouchet, R. Denoyel, Anal. Chem. 79 (2007) 9115–9121. https://doi.org/10.1021/ac071377r

[14] E.M. Renkin, J. Gen. Physiol. 38 (1954) 225–243. https://doi.org/10.1016/j.ces.2011.08.043

[15] F. Stallmach, P. Galvosas, in: G. Webb (Ed.), Annu. Rep. NMR Spectrosc., Academic Press, 2007, pp.51-131. https://doi.org/10.1016/S0066-4103(07)61102-8

[16] P.N. Sen, Concepts Magn. Reson. Part A. 23A (2004) 1–21. https://doi.org/10.1002/cmr.a.20017

[17] P.C. Carman, Flow of gases through porous media., Academic Press Inc. Publishers, New York, 1956.

[18] M.B. Clennell, Geol. Soc. Lond. Spec. Publ. 122 (1997) 299–344. https://doi.org/10.1144/GSL.SP.1997.122.01.18

[19] R. Bouchet, D. Devaux, V. Wernert, R. Denoyel, J. Phys. Chem. C 116 (2012) 5090-5096. https://doi.org/10.1021/jp210614h

[20] V. Wernert, R. Bouchet, R. Denoyel, Anal. Chem. 82 (2010) 2668–2679. https://doi.org/10.1021/ac902858b

[21] F. Gritti, G. Guiochon, J. Chromatogr. A. 1227 (2012) 82–95. https://doi.org/10.1016/j.chroma.2011.12.065

[22] F. Gritti, G. Guiochon, J. Chromatogr. A. 1280 (2013) 35–50. https://doi.org/10.1016/j.chroma.2013.01.022

[23] P. DePhilipps, A. M. Lenhoff, J. Chrom A. 883 (2000) 39-54. https://doi.org/10.1016/S0021-9673(00)00420-9

[24] L. Hagel, M. Östberg, T. Andersson, J. Chromatogr. A. 743 (1996) 33–42. https://doi.org/10.1016/0021-9673(96)00130-6

[25] E.P. Barrett, L.G. Joyner, P.H. Hallenda, J. Am. Chem. Soc. 73 (1951) 373-380. https://**doi.org/**10.1021/ja01145a126

[26] H.L. Weissberg, J. Appl. Phys. 34 (1963) 2636–2639. https://doi.org/10.1063/1.1729783

[27] J. Comiti, M. Renaud, Chem. Eng. Sci. **1989**, *44*, 1539-1545. https://doi.org/10.1016/0009-2509(89)80031-4

[28] E. Maure, M. Renaud, *Chem. Eng. Sci. 1997, 52, 1807-1817. https://doi.org/10.1016/S0009-2509(96)00499-X*

[29] B.P. Boudreau, Geochim. Cosmochim. Acta. 60 (1996) 3139–3142. https://doi.org/10.1016/0016-7037(96)00158-5

[30] S. Khirevich, A. Höltzel, A. Daneyko, A. Seidel-Morgenstern, U. Tallarek, J. Chromatogr. A. 1218 (2011) 6489–6497. https://doi.org/10.1016/j.chroma.2011.07.066

[31] H. Wang, F. Willot, M. Moreaud, M. Rivallan, L. Sorbier, D.Jeulin, Oil & Gas Science and Technology–Rev. IFP Energies nouvelles. 72 (2017) 8-25. https://doi.org/10.2516/ogst/2017002

[32] H. Kobayashi, D. Tokuda, J. Ichimaru, T. Ikegami, K. Miyabe, N. Tanaka, J. Chromatogr. A. 1109 (2006) 2–9. https://doi.org/10.1016/j.chroma.2005.11.053

[33] T.F. Johnson, P.R. Levison, P.R. Shearing, D.G. Bracewell, J. Chrom. A, 1487 (2017) 108-115. https://doi.org/10.1016/j.chroma.2017.01.013

[34] K. Hormann, V. Baranau, D. Hlushkou, A. Höltzel, U. Tallarek. New J. Chem. 40 (2016), 4187-4199. https://doi.org/10.1039/c5nj02814k

[35] D. Hlushkou, A. Svidrytski, U. Tallarek, J.Phys.Chem.C 121 (2017), 8416 – 8426. https://**doi.org/**10.1021/acs.jpcc.7b00264

[36] R. S. Maier, M. R. Schure, Chemical Engineering Science 185 (2018) 243–255. https://doi.org/10.1016/j.ces.2018.03.041

[37] F.Gritti, J. Chrom. A 1485 (2017)70-81. https://doi.org/10.1016/j.chroma.2017.01.030

[38] M.P. Hollewand, L.F. Gladden, Chemical Engineering Science 50 (1995) 309-326. https://doi.org/10.1016/0009-2509(94)00218-G

[39] D.J. Richard, A.M. Striegel, J. Chromatogr. A 1217 (2010) 7131-7137. https://doi.org/10.1016/j.chroma.2010.09.021

[40] S. Beckert, F. Stallmach, R. Bandari, M. R. Buchmeiser, Macromolecules 43 (2010) 9441–9446. https://doi.org/10.1021/ma101992c

List of figures

Figure 1 a) Mercury intrusion-extrusion curves of porous and shell-porous particles and monoliths b) Pore size distribution obtained from Hg c) Nitrogen adsorption-desorption isotherms at 77 K of porous and shell porous particles and monoliths d) Pore size distribution determined from the desorption curve by applying BJH method e) Partition coefficient Kd obtained from ISEC f) Pore size distribution obtained from ISEC

Figure 2. ISEC measurements of the a) total porosities and b) particle (in the porous zone for the core-shell column) porosities obtained for each polymer

Figure 3. Total tortuosities of silicas and alumina as a function of the total porosity determined by electrical measurements. Fit with the Maxwell model

Figure 4. a) Examples of peak shape for the peak parking method for (a) Toluene and (b) a intermediate size molecule (polymer P5) for the porous-shell silica c) Peak variance as a function of the parking time given as example for the porous-shell column (similar curves are obtained for the three other columns) d) Plots of the ratio of the experimental effective diffusivity and the molecular diffusivity (D_{eff}/D_m) versus the ratio of molecular size and mesopore size (r_m/r_p). Fit with the Maxwell equation

Figure 5. Apparent total tortuosity of the solids obtained by PP method versus the ratio of molecular size and mesopore size (r_m/r_p)

Figure 6. Plots of the ratio of the intraparticle diffusion in the porous zone and the molecular diffusion coefficient (D^{pz}/D_m) versus the ratio of molecular size and mesopore size (r_m/r_p)
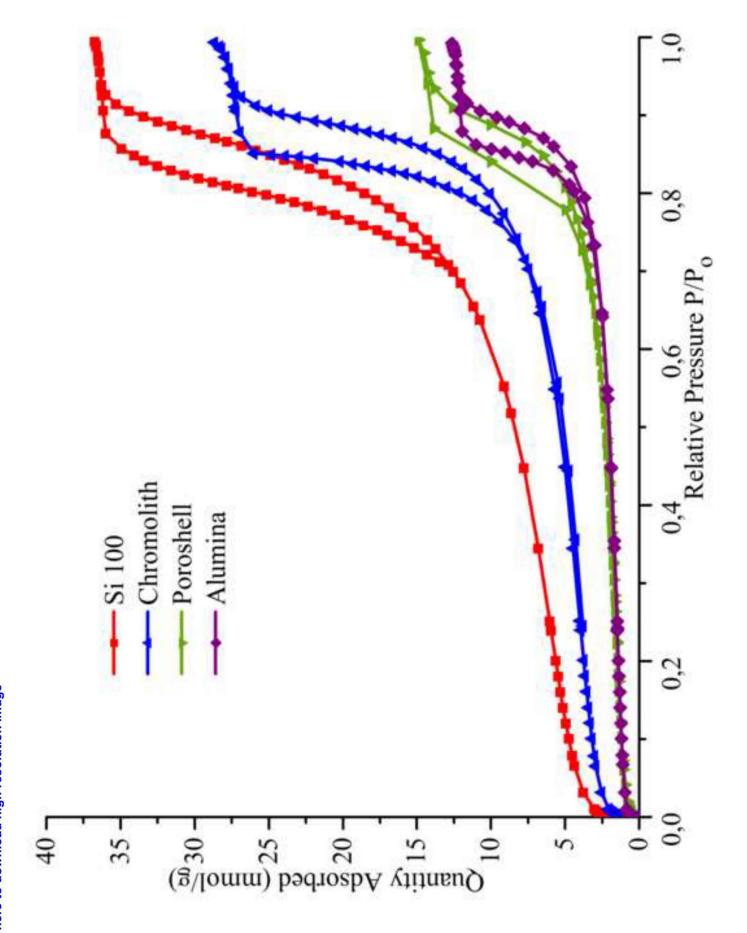
Figure 7. Particle tortuosity obtained from the PP method and by electrical measurements as a function of particle porosity. Fit with the Weissberg equation by using the p value obtained by electrical measurements
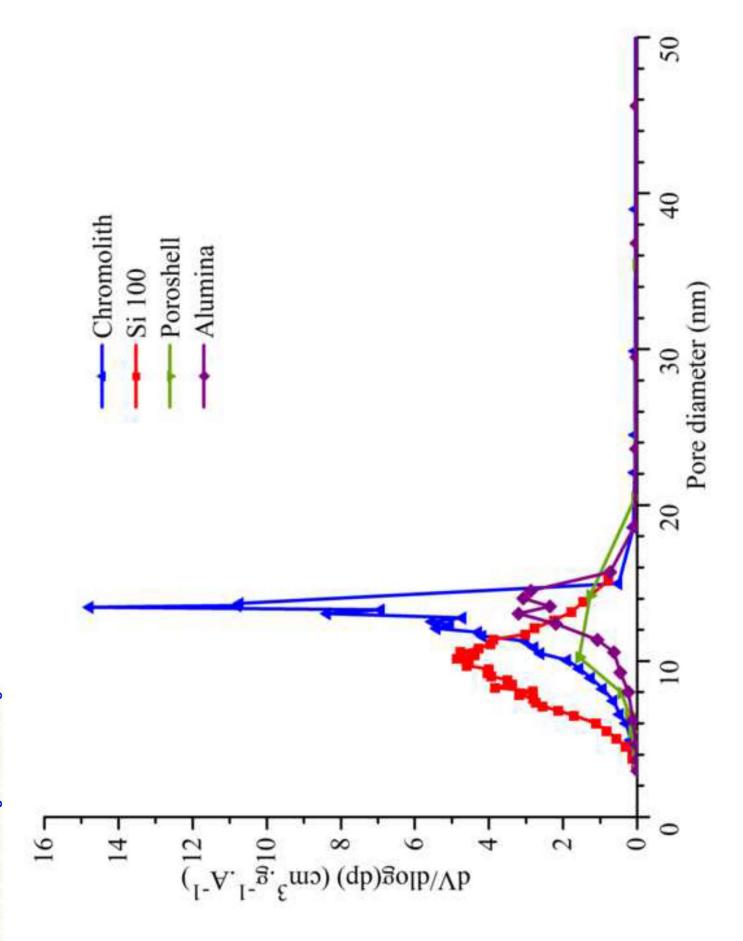
Legend: Chromolith, Si 100, Poroshell, Alumina

X-axis: Pore diameter (nm)
Y-axis: log differential intrusion (mL.g⁻¹)

Table(s)

List of tables

Table I : Geometrical characteristics of the considered particle types, including the column's dimension, particle diameter d'_p, the ratio ρ between the diameter of the core d_c and the diameter of the particle and the mean pore diameter (d_p) (data taken from manufacturers documentation)

	Samples	Suppliers	Support	Column's dimension length [mm] I.D. [mm]	d'_p (μm)	$\rho=d_{core}/d'_p$	d_p (nm)
Totally porous particles	Lichrospher Si 100	Merck	silica	250x4	5	0	10
	Chromegasphere Alumina	ESI	alumina	150x4.6	5	0	13
Core-shell particles	Poroshell 120	Agilent	silica	150x4.6	4	0.625	12
Monoliths	Chromolith Si	Merck	silica	100x4.6	-	0	13

Table II. Molecular weights (Mw), polydispersity (PDI), bulk diffusion coefficient D_m obtained by TDA for the smallest polymers (Toluene, P01, P02 and P03) and by DLS for the others polymers (P04 to P12) of the solutes used in ISEC and hydrodynamic radii r_m calculated with Stoke Einstein equation (taken from Wernert et al 2010 [20])

Polymer code	Molecular weight $M_w^{(1)}$ /g mol^{-1}	PDI[1]	Molecular diffusion coefficient D_m (TDA and DLS measurements) [2] /m^{2}s^{-1}	probe radius r_m [2] /nm
toluene	92		$2.15 \cdot 10^{-9}$	0.22
P01	162	1.00	$1.51 \cdot 10^{-9}$	0.31
P02	690	1.09	$7.10 \cdot 10^{-10}$	0.67
P03	1380	1.05	$5.00 \cdot 10^{-10}$	0.95
P04	3250	1.05	$3.19 \cdot 10^{-10}$	1.43
P05	8900	1.03	$2.04 \cdot 10^{-10}$	2.36
P06	19100	1.03	$1.33 \cdot 10^{-10}$	3.62
P07	33500	1.03	$8.73 \cdot 10^{-11}$	5.50
P08	96000	1.04	$5.08 \cdot 10^{-11}$	9.44

P09	243000	1.03	$3.19. \ 10^{-11}$	15.02
P10	546000	1.02	$2.10. \ 10^{-11}$	22.84
P11	827000	1.08	$1.65. \ 10^{-11}$	29.09
P12	1850000	1.05	$1.12. \ 10^{-11}$	42.90

(1) Given by supplier (2) Wernert *et al* 2010 [20]

Table III. Structural properties of the columns including the total porosity ε_t, the external porosity ε_e, the porosity of the porous zone ε_{pz} and the pore diameter (d_p) obtained by ISEC, mercury intrusion porosimetry and N_2 adsorption. The macropore diameter is obtained by Hg porosimetry

Materials	ISEC				Hg porosimetry					N_2 adsorption	
	ε_t	ε_e	ε_{pz}	d_p (nm)	ε_t	ε_e	ε_{pz}	d_p (nm)	d_{macro} (µm)	ε_{pz}	d_p^a (nm)
Lichrospher Si100	0.80	0.37	0.69	15.4	0.77	0.36	0.64	5.5 and 14	1.85	0.70	10.2
Poroshell	0.67	0.39	0.60	15.8	0.62	0.37	0.53	9.94	0.88	0.53	11.0
Chromolith	0.93	0.69	0.77	14.8	0.87	0.63	0.65	10.10	1.48	0.69	11.2
Chromegasphere Alumina	0.73	0.42	0.53	18.4	0.71	0.38	0.52	12.48	1.29	0.53	13.0

[a] from desorption branch

Table IV Tortuosities obtained by electrical measurements : total tortuosity (τ_t) for monolith, intraparticle tortuosity (τ_p) for spherical particles and by the PP method : total tortuosity (τ_t) obtained with toluene, external tortuosity (τ_{ext}) obtained for molecules having a size larger than the pore size, and the intraparticle tortuosity (τ_p) obtained with toluene. The intraparticle tortuosity is calculated from the Maxwell model and the p values are calculated from the Weissberg equation.

columns		tortuosity (conductivity)			Tortuosity obtained by PP method					
		τ_t	τ_p		$\tau_{t\ (toluene)}$	External tortuosity		Particle tortuosity (toluene)		
			τ_p	p		τ_{ext}	p	τ_p	p	
Totally porous particles	silica	-	1.6	1.6	1.1	1.4	0.4	1.6	1.6
	alumina	-	1.8	1.3	1.05	1.4	0.4	1.8	1.3
porous-shell particles	silica	-	2.3	2.5	1.2	1.4	0.4	2.7	3.3
Monoliths	silica	1.13	-	-	1.09	1.1	0.3	1.6	2.3